2013-04-23

Regulated Emissions from a High Efficiency Spark-Ignition with Maximum Engine Power at or Below 19 KW

Travis J. Mackey
University of Miami, travisjmackey@gmail.com

UNIVERSITY OF MIAMI

REGULATED EMISSIONS FROM A HIGH EFFICIENCY SPARK-IGNITION ENGINE WITH MAXIMUM ENGINE POWER AT OR BELOW 19KW

By

Travis Jamal Mackey

A THESIS

Submitted to the Faculty
of the University of Miami
in partial fulfillment of the requirements for
the degree of Master of Science

Coral Gables, Florida

May 2013

UNIVERSITY OF MIAMI

A thesis submitted in partial fulfillment of
the requirements for the degree of
Master of Science

REGULATED EMISSIONS FROM A HIGH EFFICIENCY SPARK-IGNITION ENGINE WITH MAXIMUM ENGINE POWER AT OR BELOW 19KW

Travis Jamal Mackey

Approved:

_____	_____
Michael R. Swain, Ph.D. Associate Professor Mechanical & Aerospace Engineering	M. Brian Blake, Ph.D. Dean of the Graduate School
_____	_____
Matthew N. Swain, Ph.D. President Analytical Technologies Incorporated Engineering	Singiresu S. Rao, Ph.D Professor Mechanical & Aerospace

MACKEY, TRAVIS JAMAL (M.S., Mechanical Engineering)
Regulated Emissions from a High Efficiency (May 2013)
Spark-Ignition Engine with Maximum Engine Power at or Below 19KW

Abstract of a thesis at the University of Miami

Thesis supervised by Professor Michael R. Swain.
No. of pages in text. (42)

Previous research has developed a set of high efficiency generator engines converted from a stock automobile engine. These all employed different variations of squish and swirl along with running at a high compression ratio in their design. The stock engine was a 1.6L four cylinder engine fueled by propane and configured for lean operation. These modifications produced a 36.8% reduction in EPA cycle fuel consumption.

The objective of this research was to determine whether this high efficiency engine could meet stringent regulated emissions standards set by the EPA. By varying spark advance and air-fuel ratio, an engine was created to meet EPA standards which had an increase of 1.7% in fuel consumption over the high efficiency engine without having to use a catalyst. Therefore, this engine could be produced cheaply and sold in the United States or abroad.

Acknowledgement

I would like to thank Dr. Michael Swain for his continuous guidance and support. Without him, none of this would have been possible.

I would like to thank Dr. Matthew Swain for his help with experimental and data preparation.

I would like thank my family especially my aunt, Dr. Flora Mackay, for their constant encouragement and support. Without their sacrifices this could not have been possible.

I would also like to thank my friends for all their support.

TABLE OF CONTENTS

LIST OF FIGURES

LIST OF TABLES

Nomenclature

A = Total orifice area expressed in square feet

ACFM = Actual Cubic Feet per Minute

BTE = Brake Thermal Efficiency

C = Orifice Coefficient

CA = constant

CO = Carbon Monoxide

HC = Hydrocarbons

i = test interval number

K = Constant = 4,005 when P is expressed in In. of Water

$\dot{m}$ = mass flowrate in grams per hour

N = number of test intervals

NO_x = Oxides of Nitrogen

P = Pressure differential across the orifice

$\overline{P}$ is the mean steady-state power over the test interval

p = pressure in the humid air (Pa*)*

P_{act} = absolute pressure at the actual level (psia)

p_a = atmospheric pressure of moist air (Pa, psi)

p_{abs} = wet static absolute pressure at the location of your relative humidity measurement

P_{air} = Air Pressure in psi

p_{H20} = water vapor pressure at 100% relative humidity at the location of your relative humidity measurement

P_{sat} = Saturation pressure at the actual temperature (psi)

P_{std} = Standard absolute air pressure (psia)

P_{vapour} = Vapour Pressure in psi

p_w = partial pressure of water vapor in moist air (Pa, psi)

Q = Volume flow rate in cubic feet per minute (CFM)

Q_{dry} = Dry Volume flow rate in cubic feet per minute (CFM)

Q_{wet} = Wet Volume flow rate in cubic feet per minute (CFM)

R = Universal Gas Constant in Joules per Kilogram Kelvin

R_a = 286.9 - the individual gas constant air (J/kg K)

R_w = 461.5 - the individual gas constant water vapor (J/kg K)

RH % = relative humidity

SCFM = Standard Cubic Feet per Minute

T = Ambient Temperature in Kelvin

T_{act} = Actual ambient air temperature (^oR)

T_{sat} = saturation temperature of water at measured conditions, K

T_{std} = Standard temperature (^oR)

V = Velocity in feet per minute (fpm)

v = specific volume of moist air per mass unit of dry air and water vapor (m^3/kg)

WF = weighting factor for the test interval as defined in the standard-setting part

x = specific humidity or humidity ratio (kg/kg)

x_{H20} = amount of water in an ideal gas

ρ = Air Density in Kilogram per meter cubed

Φ = Actual relative humidity

Chapter 1

Introduction

Electrical generators have become popular because they provide a portable instant supply of electrical power at consumer demand. They were mostly used in critical need applications such as hospitals and airports, but have found their way into homes frequented with power outages or homes in remote locations. With the increase in popularity of this type of engine, people have started to assess the effect on the environment which has resulted in stringent government regulations for engine emissions.

The objective of this investigation was to develop an engine that would meet these stringent emissions standards regulated by the environmental protection agency and produce as high efficiencies as possible. The principle concept was to minimize expense by rebuilding an older automobile engine and avoiding the purchase of a brand new production engine. This automobile engine was used to develop and optimize a genset for both efficiency and to comply with EPA regulations. This presents a less expensive way to get a more efficient engine particularly to act as an electrical generator.

Emissions and efficiency data are deemed necessary for production and sale of any engine. This research has been driven mainly by government legislation requiring ever lower emission standards and improved fuel economy (Baker and Watson). The emissions data is important because any engine to be sold in the United States must meet a certain level of pollution set by the EPA. This inherently affects the cost of the engine as more money may need to be invested in the development of a catalyst to meet these standards. Also, it is essential to determine the efficiency of the engine because

consumers typically assess how many times they will have to buy fuel for a certain power output. This characteristic becomes more vital in areas with limited access to a fuel supply.

The engine examined for this investigation was a 1.6L Single Overhead Cam Spark Ignition Engine with a bore of 79 mm and a stroke of 83.6 mm fueled by liquid propane at an RPM of 1800 and max BMEP of 110 PSI. This engine would produce electrical power of about 15 kW to 17.5 kW. At full load, a generator of this size typically operates with 85% efficiency and 2% slippage. Therefore, the desired engine size to produce about 17.6 kW to 20.6 kW of electricity needed to produce about 20kW to 21.7 kW. Some of this power is also needed for cooling purposes. Since this engine produced below 19 KW of total power, this particular engine was classified as a small non handheld non road spark ignition engine according to EPA Title 40, Code 1054.

This code also outlined the emission standards this engine would be required to meet. Table 1 depicts these standards based on the size of engine displacement. The code classifies any engine with a total displacement at or larger than 225 cc as Class II. Hence, this engine had to meet this standard if it was to be produced and sold here in the United States.

Engine displacement class	$HC+NO_X$	Primary CO standard	CO standard for marine generator engines
Class I	10.0	610	5.0
Class II	8.0	610	5.0

Table 1: EPA Emissions standards in g/KW-hr

Examination of Engine Design

The conversion of an automobile engine to be used in a generator opens several avenues to improve engine efficiency. Automobile engines are designed to sustain operation over a wide range of rpms. Generators typically run at a constant and much lower rpm. This lower rpm produces significantly reduced inertial forces in mechanical moving parts which allow for the use of lighter valve train springs, smaller bearings, lighter pistons, and lighter connecting rods. These changes decrease the amount of friction. Thus, there are less frictional losses and an improved efficiency.

These reduced inertial forces and friction are quantified by frictional mean effective pressure (Bishop). These helped to improve efficiency most at light loads. The crankshaft main bearing main bearing size was approximately 49.9 mm in diameter and 17.6 mm in length. The journal bearing size was about 39.9 mm in diameter and 17.1 mm in length. Cast iron connecting rods were used which were 139.9 mm in length and 418 g in weight. The low friction ring package consisted of a 1mm steel gas nitrated barrel face top compression ring and a 1.2 mm cast iron phosphate coated tapered-face napier scraper ring. The three piece oil ring was 2.8 mm wide and used a stainless steel flex vent spacer with gas nitrated rails.

A basic representation of the Otto Cycle is shown below in equation 1. It depicts that high efficiency results from a combination of a high compression ratio and high ratio of specific heats.

$$n = 1 - \frac{1}{CR^{(k-1)}} \qquad (1)$$

Thus, another important design consideration was the use of a high compression ratio which was possible due to the high octane of LPG. The engine ran at a compression

ratio of 12.7 to 1. This was chosen as tests from operation with 12.2:1 compression ratio indicated that there would be no problem with knock at 12.7. Running at high compression ratio increases the flame speed of the lean LPG mixture.

However, an increase in compression ratio leads to an increase in the surface to volume ratio which produces more heat losses. This was where establishing the appropriate stroke and bore was essential as it helped to reduce the surface to volume ratio. For a 1.6L four-cylinder engine with a hemispherical combustion chamber, table 2 depicts how the surface-to-volume ratio varies with compression ratio and stroke length. It shows that a long stroke would be needed to achieve a low surface-to-volume ratio with the high compression ratio that the engine utilized. In this table, the surface-to-volume ratio is given in units of cm^{-1}.

	Compression Ratio						
Stroke (mm)	**9**	**10**	**11**	**12**	**13**	**14**	**15**
85.0	2.12	2.33	2.55	2.88	2.99	3.22	3.44
80.0	2.21	2.45	2.68	2.92	3.15	3.39	3.63
75.0	2.33	2.57	2.83	3.08	3.34	3.59	3.85
70.0	2.46	2.73	3.00	3.27	3.55	3.83	4.10
65.0	2.61	2.90	3.20	3.50	3.80	4.10	4.40

Table 2: Surface-to-Volume Ratio as a function of Stroke and Compression Ratio

An increase in compression ratio causes an increase in the amount of HC's (hydrocarbons) and NO_x as well. The HC's increase because the only way to increase the compression ratio is to increase the surface-to-volume ratio. This increase in surface produces more unburned HC's. It also produces a cooler exhaust resulting in less oxidation in the exhaust so the HC's increase. NO_x increases due to an increase in peak cycle temperatures.

Since there was a high heat transfer coefficient due to the swirl and motion of the

gas, a lower surface to volume ratio was needed in the combustion chamber to help resolve this issue. The intent in this part of the design was to minimize the amount of heat loss by reducing the area enclosing a certain volume. Forged flat top pistons were custom made to minimize the surface-to-volume ratio. These pistons were made with the 79.0 mm bore and 20 mm wrist pins which weighed 280 g including rings. Valve reliefs amounting to a total of 0.5 cc were cut into the piston head on both the intake and exhaust as shown in figure 1.

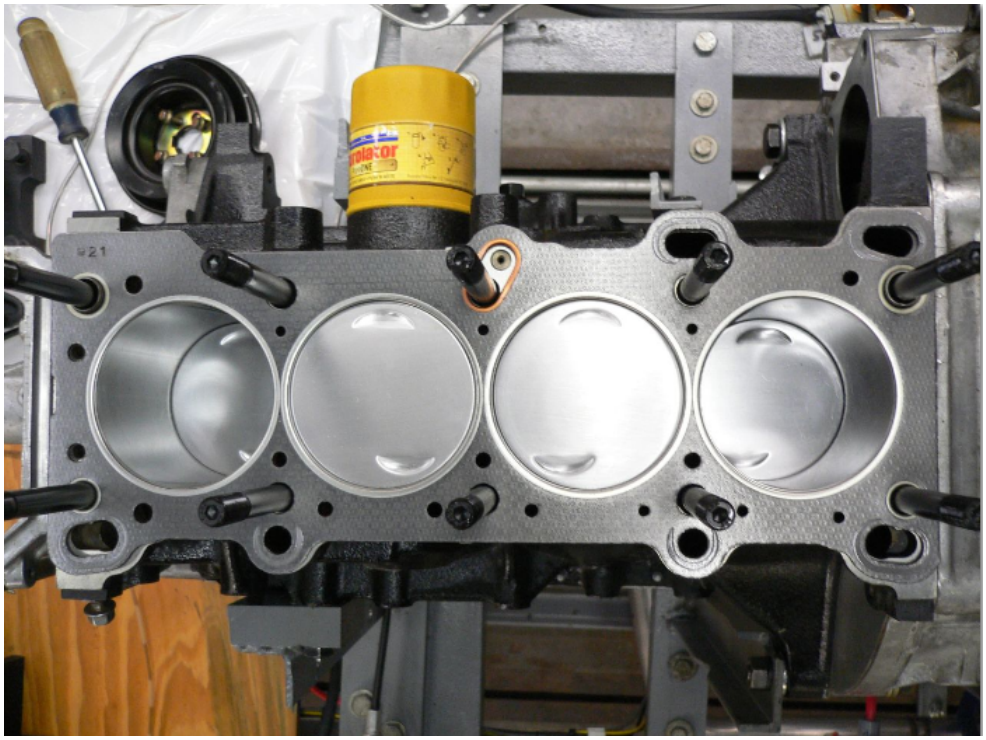

Figure 1: Installed Custom Forged Flat-Top Pistons with Valve Relief

Since heat loss is reduced, the temperature of the entire cycle was increased resulting in an increase in NO_x. However, this problem was overcome by the use of the lean mixture. Lean operation lowers the temperature of the entire cycle by minimizing the temperatures of the working fluids and gives a larger ratio of specific heats which correlates to an increase in efficiency as shown in equation 1. Lean mixtures also lower

the pumping mean effective pressure (PMEP) by creating a high intake manifold pressure for similar fuel flow rates. In terms of emissions, lean operation decreases both carbon monoxide (CO) and nitric oxide (NO) emissions while maintaining good fuel economy (Quader).

One of the biggest problems associated with lean operation is that it decreases the flame speed which results in increased time losses. To fix this, additional augmentation of the flame speed utilizing squish and swirl as shown in figure 2 were also implemented in the design of this engine. These included a super high swirl rate at a flow rate averaged swirl ratio of 3.2 with a squish area of 36%. This purpose for using such a high rate of swirl was not only to help with flame propagation, but also to make it possible to meet emissions standards without having to use a catalyst, ultimately producing a reduction in the cost of the engine. This design had to be carefully selected as too much swirl would result in high rates of heat loss which would produce a loss in efficiency greater than the increase in efficiency gained from reduced time losses. These high rates of heat loss occur as the gas is moving rapidly past the cylinder wall which causes an increase in the heat transfer coefficient from gas to the wall. Additionally, too much squish can quench flame initiation.

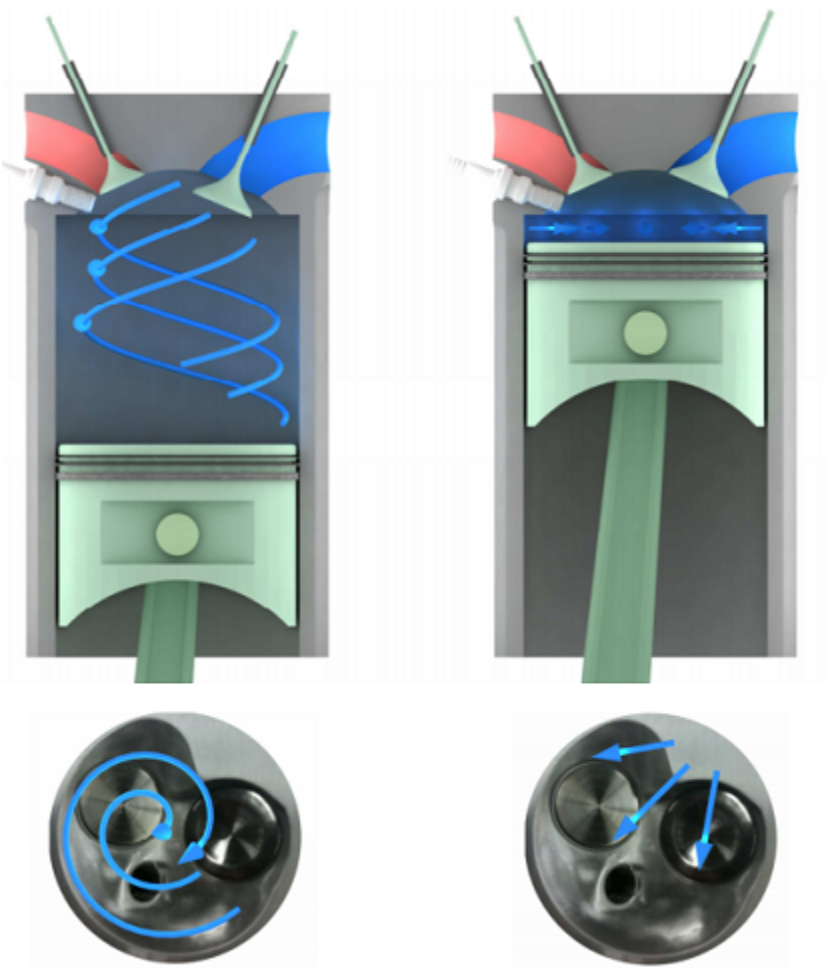

Figure 2: Depiction of Swirl (left) and Squish (right).

Formation of Exhaust Emissions

Most people attribute the majority of a city's air pollution to mass production from major manufacturing industries while completely ignoring the effects of the engine used in their personal vehicle or generator. Although significantly lower than air pollution from industry individually, adding up the pollution from millions of vehicles within a city does significantly impact the air quality of the atmosphere. With the vast increase in the amount of internal combustion engines that are used in everyday life, concern has been drawn to their contribution to air pollution.

As a direct result of the combustion process employed in an internal combustion engine, several unfavorable emissions are produced which require monitoring. For this reason the EPA has established National Ambient Air Quality Standards (NAAQS) to regulate these emissions. The NAAQS defines levels of air quality that are necessary, with a reasonable margin of safety, to protect public health (primary standard) and public welfare (secondary standard) from any known or anticipated adverse effects of pollution.

The emissions of primary concern are carbon monoxide (CO), unburned hydrocarbons (HC), and oxides of nitrogen (NO_x), primarily nitric oxide and nitrogen dioxide. These all contribute to air pollution and produce detrimental occurrences such as smog, acid rain, and respiratory problems. Another engine emission of concern that is not regulated is carbon dioxide which is believed to be a principal cause of global warming.

There are several forms of emission control in an internal combustion engine. The engine operating conditions such as air-fuel-ratio, ignition timing, and exhaust gas recirculation (EGR) can be varied. The combustion process can be enhanced with the use of more expensive and complex equipment such as the fuel injectors, oxygen sensors, and

on-board computers. Also, a catalyst can be used to breakdown emissions in the exhaust.

For this research effort, emissions standards were met by varying only spark advance and the air-to-fuel ratio. This was done to simplify to cost of producing the engine. Figure 3 shows the expected trend of emissions as the mixture is made leaner and leaner as done in this research.

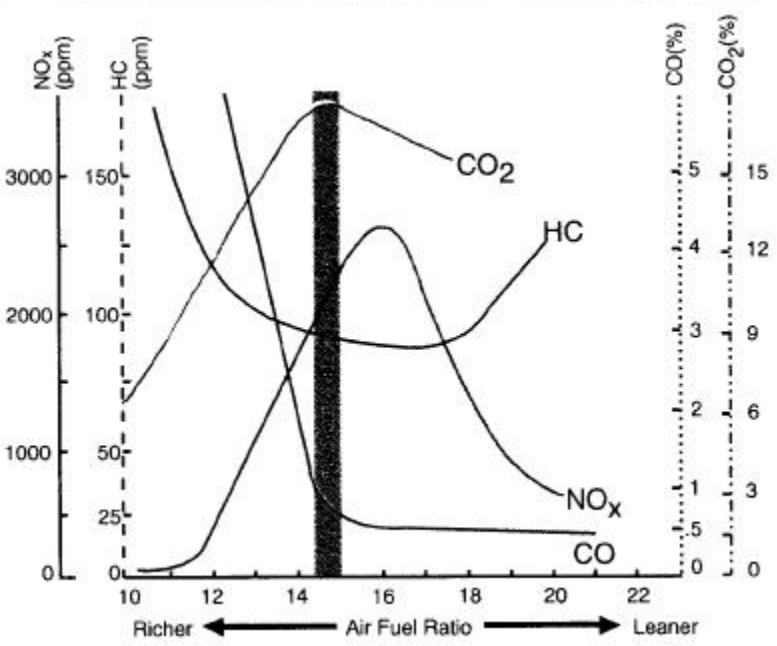

Figure 3: Expected Emissions Pattern as a Function of Air-Fuel Ratio

Hydrocarbon Formation

Hydrocarbons typically form as a result of fuel that didn't fully burn during the combustion process. For this research, pure propane was used which initially consists of 3 carbon atoms and 8 hydrogen atoms prior to combustion. General motors conducted a study into the formation of hydrocarbons. This study outlines three possible explanations as to why some of the fuel remains unburned, thus creating these hydrocarbons. It explains that one possible reason some of the fuel is not burned in the combustion chamber is because of excessive residual gas dilution or quenching of the flame near the

wall of the chamber. Another reason for the formation of hydrocarbons comes as some of the fuel escapes the reaction when the flame propagates through the chamber and creates a reaction during the expansion and exhaust portions of the cycle. Finally, some of the fuel that fails to burn is retained in the chamber in the residual gases. (Daniel).

Other possible causes for the formation of hydrocarbons that were not covered by this study include fuel that is unburned because it is pushed into tiny crevice volumes in the combustion chamber. These are miniature areas in the combustion chamber where the flame cannot enter. Typical crevice volume areas are around the pistons rings, threads in the spark plug, valve seats, and the head gasket. These all attempt to explain how hydrocarbons are formed, but more research is still being done to explain this phenomenon as the formation of hydrocarbons remains unpredictable.

NO_x Formation

Nitrogen is an inert gas which constitutes about 79% of earth's atmosphere. Nitrogen does not typically react during the combustion process. Only at high temperature and pressure conditions in the engine does nitrogen react with atoms of oxygen to produce various forms of nitrogen oxides. This reaction rate tends to be relatively slow, especially at temperatures below 2000K. Hence, NO_x formation at low temperatures becomes negligible.

Nitrogen varies with changes in air-fuel ratio as shown in figure 3. It depicts that NO_x is relatively low at rich mixtures and increases as the mixture becomes leaner. This is due to the fact that there is not enough oxygen available in rich mixtures to form these oxides of NO_x. Thus, as more oxygen becomes available, NO_x is expected to increase.

However, after a certain point the excess air drops the peak temperatures and NO_x begins to decrease again.

CO Formation

Carbon monoxide is formed as a result of incomplete combustion. It comes from the fuel that is not fully oxidized during the combustion process. CO, like other regulated emissions, is also very dependent on the air-to-fuel ratio. Figure 3 shows that CO is prevalent at rich mixtures, but at a minimum in lean mixtures. This is primarily accounted by the lack of oxygen available in rich mixtures to completely oxidize all of the carbon atoms in the fuel. However, at lean mixtures, there is more than enough oxygen to complete oxidation of the carbon atoms to carbon dioxide. The greatest occurrence of CO emissions comes at engine start-up where the mixture tends to be richer than at normal operation.

Rates of CO formation are also reliant on temperature. Even in lean mixtures when there is enough oxygen present to complete oxidation, high peak temperatures produce dissociation which causes the carbon dioxide to break off to form CO. At low temperatures, there is little formation of CO. This is because at lower temperatures, the reaction rate is slower so CO concentrations remain low. The gas temperature is low enough that the reaction rate from CO to carbon dioxide is slow enough to free small amounts of CO during the expansion stroke. This is observed in lean operation. Thus, for this research effort it was predicted that CO would not be problematic due to lean operation of the engine.

Chapter 2

General Equipment and Procedure

A Superflow water-brake dynamometer was used to measure the torque produced during testing. This torque rotated the engine crankshaft. An Ametek strobe was used to measure the rpm of the crankshaft. Spark Advance was controlled using a Haltech engine control unit (ECU). Measurements of incoming air flow rate was taken from a Meriam Laminar Flow element. The pressure difference was recorded from the Meriam Inclined Manometer. Fuel flow rate was measured using a Cox rotameter. The exhaust temperature was recorded for each cylinder from thermocouples attached to a spacer plate between the exhaust ports and exhaust manifold which allowed the thermocouples to be set up directly in the exhaust flow. A non-dispersive gas analyzer (NDIR) was used to record the amount of emissions present in the exhaust. The hydrocarbon used to calibrate the NDIR was propane. The air-fuel ratio was also taken from an oxygen sensor placed in the exhaust. Table 3 lists information about all instruments used. These instruments are shown in the Appendix.

Measurement Apparatus	Make and Model	Accuracy
Dynamometer	Superflow D-516	±.2% Reading
Strobe	Ametek Digistrobe III 1965	±1% Reading
Laminar Flow Element	Meriam 50 MC2-2P	±.65% Reading
Inclined Manometer	Meriam 40OHE35WM	
NDIR Gas Analyzer	Ferrett 16 Gas Link II	±2% Reading
ECU	Haltech E8	
Rotameter	Cox 129-287	±0.5% Reading
Oxygen Sensor	Innovative LM-2	
Thermocouples	Omega OMEGACLAD KMQXL-032G-6	
Ambient Pressure Gauge	Oakton Aneroid Manometer	

Table 3: Measurement Instruments Information

Fuel was delivered to the engine using a standard minor diameter radial inlet venturi gaseous fuel mixer as shown in Figure 4. This mixture was passed through a 175 cc pre-chamber before a transition through a 6.4 cm^2 orifice into the intake manifold. This was used in an effort to achieve better cylinder to cylinder fuel distribution over the stock engine. This intake geometry created a 20 mm mercury intake manifold vacuum at wide open throttle.

Figure 4: Fuel Mixer

Before any testing or data measurements were done it was essential to allow the engine to warm up to a consistent operating condition which was based on oil temperature and pressure. This usually took approximately 20 minutes to attain this condition. If this were not done, data taken would be inaccurate due to changes in friction that result from a decrease in oil viscosity as oil temperature increases. Changes in friction directly produce changes in the power output of the engine.

This engine maintained stable operating conditions at an oil pressure and temperature of about 27 psi and 185°F. It was initially set at 25° spark advance and 1800 rpm. To determine best efficiency and emissions compliance, data was taken at different torques, spark advance, and air-fuel ratios. For emissions compliance, the EPA requires data be taken at 100, 75, 50, 25, 10, and 0 percent load. Thus, spark advance and air-fuel ratio were varied for best efficiency and compliance with emissions standards.

Emissions Calculations

Table 1 was used to establish whether this engine would meet the emissions standards set by the EPA. By EPA classifications, the engine used in this research is defined as Class II as it relates to nonhandheld engines with total displacement at or above 225 cc.

Engine displacement class	$HC+NO_X$	Primary CO standard	CO standard for marine generator engines
Class I	10.0	610	5.0
Class II	8.0	610	5.0

Table 1: EPA Emissions standards in g/KW-hr

To measure concentrations of emissions coming out of the exhaust an NDIR (non-dispersive infrared) gas analyzer was utilized. However, a problem existed in that the NDIR gas analyzer reported emissions in parts per million. Therefore, from the data reported by the analyzer, a conversion to grams per KW-hr had to be established to compare with EPA standards defined in table 1 and to draw accurate conclusions from the results taken.

After ensuring that measurements made were as accurate as possible, the first step taken in trying to convert parts per million exhaust to grams per KW-hr was to calculate the volume flow rate of the incoming air. The inclined manometer utilized a square inch orifice to measure this flow rate and had a calibrated value of 41 SCFM at 7.02 inches of water at standard temperature and pressure (70°F and 14.696 psia). Since testing was not conducted at these standard conditions, equation 2 was used to derive the actual flow rate given the actual condition present in the room at the time of testing (Engineering

Toolbox).

$$ACFM = SCFM\,[P_{std} / (P_{act} - P_{sat}\,\Phi)](T_{act} / T_{std}) \quad (2)$$

Since the value of the actual flow rate at the calibrated pressure was known, the next step was to find the flow rate of air through the intake at the measured pressure drop. To determine air flow through the orifice the following equations were used:

$$V = CK\sqrt{P} \quad (3)$$

Equation 3 was used to calculate the flow coefficient through the orifice. This was important as the flow coefficient would remain constant throughout the entire experiment. However, the velocity of the incoming air was unknown. Therefore, equation 4 was used to substitute for velocity.

$$Q = AV \quad (4)$$

Since the area and the flow coefficient remained constant and since they were both unknown, they were calculated by combining the two constants to form a coefficient called *CA*. This constant was calculated using the calculated value for ACFM and the calibrated value for pressure. Combining equations 3 and 4 produces equation 5 which gives a value for the total flow rate of wet air coming in.

$$Q_{wet} = CAK\sqrt{P} \quad (5)$$

Since the mass flow rate in of dry air would have to be calculated later on, at this point it was also important to calculate the volume flow rate of dry air in. This was done by the following relation:

$$Q_{dry} = CAK\sqrt{P} * \frac{P_{air} - P_{vapour}}{P_{air}} \quad (6)$$

In order to be able to calculate the mass flow rate of dry and wet air coming into the engine it was necessary to find the air density of both wet and dry air. The density of

air was found using the ideal gas law as shown in equation 7.

$$\rho_{dry} = \frac{P_{air}}{RT} \quad (7)$$

For this equation, a value of 286.9 J/kg K was used for the universal gas constant. Then, to calculate the value of air density, factoring in the water vapor, equation 8 was utilized (Engineering Toolbox).

$$\rho_{wet} = 1/v = (p / R_a T) (1 + x) / (1 + x R_w / R_a) \quad (8)$$

Here x is:

$$x = 0.62198 p_w / (p_a - p_w) \quad (9)$$

Utilizing these equations, calculated values of the density and volume flow rate was reported for each point.

Now that the values have been determined for air density of wet and dry air and flow rate of wet and dry air, the mass flow rate was derived using equation 10.

$$\dot{m} = \rho Q \quad (10)$$

Next, it was essential to assess how much fuel was coming into the engine with this mass flow of air. The value of lambda recorded during testing allowed for the calculation of the air to fuel ratio through the balancing of the chemical equation caused by this reaction of air and propane. Equation 11 describes this process.

$$C_3H_8 + 5O_2 + 18.8N_2 \rightarrow 3CO_2 + 4H_2O + 18.8N_2 \quad (11)$$

Equation 11 assumes that the mixture is stoichiometric. For this mixture, the air to fuel ratio is 15.572. However, this is not the case. Thus, equation 11 must be re-balanced to include lambda. For example, this is done in equation 12 at $\lambda=1.255$ or $\phi = 0.8$. It is also important to note that both equations 11 and 12 account only for dry air coming in.

$$0.8\ C_3H_8 + 5O_2 + 18.8N_2 \rightarrow 2.4CO_2 + 3.2H_2O + 18.8N_2 + O_2 \qquad (12)$$

For this mixture, the air to fuel ratio becomes 19.465. Given this value, the total amount of fuel coming into the engine can be calculated. Modifying the chemical equation to include the presence of water, the following equation was obtained.

$$x_{H_2O}H_2O + 0.8C_3H_8 + 5O_2 + 18.8N_2 \rightarrow 2.4CO_2 + (3.2 + x_{H_2O})H_2O + 18.8N_2 + O_2 \qquad (13)$$

Here x_{H_2O} is:

$$x_{H_2O} = \frac{RH\% \cdot p_{H_2O}}{p_{abs}} \qquad (14)$$

Where p_{H_2O} is:

$$log_{10}(p_{H_2O}) = 10.79574 \cdot \left(1 - \frac{273.16}{T_{sat}}\right) - 5.02800 \cdot log_{10}\left(\frac{T_{sat}}{273.16}\right) + 1.50475 \cdot 10^{-4} \cdot \left(1 - 10^{-8.2969 \cdot \left(\frac{T_{sat}}{273.16} - 1\right)}\right) + 0.42873 \cdot 10^{-3} \cdot \left(10^{4.76955 \cdot \left(1 - \frac{273.16}{T_{sat}}\right)} - 1\right) - 0.2138602 \qquad (15)$$

Here, x_{H_2O} represents the total number of moles of water that was calculated by considering the partial pressures of air and water at each data point.

Finally, the last mass flow rate that needs to be taken into account is the mass flow rate of water due to humidity coming into the engine. This was calculated simply be subtracting the mass flow rate of dry air from the mass flow rate of wet air. At this point, all calculations of mass flow rate into the engine are complete.

After finding the mass flow of air, the next step was to find the total molar flow rate leaving the engine. This allows for a conversion of the emissions results given from parts per millions to grams per KW-hr. By the conservation of mass equation, it is known

that the mass flow rate in is equivalent to the mass flow rate out. Therefore, from the results of mass flow rate in, data for mass flow rate out was obtained.

The molar flow rate values seen were calculated by dividing each mass flow rate by its own molecular weight. For air a value of 28.9652 g/mol was used. For the fuel a value of 44.09592 g/mol was used. For water a value of 18.01532 g/mol was used.

Adding these together, allowed for the calculation of the total molar flow rate wet leaving the engine. Since the NDIR analyzer reported values for emissions dry, a correction was made to achieve the total molar flow rate dry that would enable proper calculations of emissions in g/hr. Using the chemical equation listed above, the following relationship was derived.

$$Total\ Molar\ FR_{dry} = \frac{2.4+18.8+1}{2.4+3.2+18.8+1+x_{H_2O}} * Total\ Molar\ FR_{wet} \qquad (16)$$

Next, by multiplying the total molar flow rate dry by the molecular weight of each emission and by the concentration given by the gas analyzer, emissions data was calculated in the desired units of g/hr.

Finally, the EPA requires a summation of a mean mass flow rate multiplied by a given weighting factor at a designated torque level divided by a summation of mean power multiplied by this weighting factor over all modes to be taken to determine whether the engine meets the standard described in table 1. This is summarized by equation 17.

$$e_{composite} = \frac{\sum_{i=1}^{N} WF_i \cdot \overline{\dot{m}_i}}{\sum_{i=1}^{N} WF_i \cdot \overline{\dot{P}_i}} \qquad (17)$$

These waiting factors were set by the EPA and defined for each mode in table 5. Here, each mode simply corresponds to a different torque level.

G2 mode No.	Torque (percent)	Weighting factors
1	100	0.09
2	75	0.2
3	50	0.29
4	25	0.3
5	10	0.07
6	0	0.05

Table 4: EPA Emissions weighting factors at different loads

Chapter 3

Evolution of Engine

The engine selected for this research was a 1.6L four-cylinder B6/B6E two valve single overhead cam engine designed by Mazda, but also manufactured or used by Ford and Kia. This made parts relatively easy to find since they were in such abundance. However, the cylinder head chosen was from a smaller 1.3L engine in the same family. This head was able to be swapped out with the 1.6L head and used by simply making changes to the position of the water jacket. This allowed the use of a higher compression ratio without the need to weld extra aluminum to the combustion chamber. Additionally, the inlet swirl could be modified due to the small size of the intake system which produced a Mach index number of 0.20 to 0.22 at 1800 rpm with an intake valve head diameter of 31.75 mm and an intake port diameter of 26 mm. Another reason the Mazda engine was chosen was because it already had reasonably high swirl for a gasoline engine which would be needed in this research effort for lean operation.

Table 5 lists the three heads that were developed and tested for this research effort. The three heads were the Low Swirl (LS), High Swirl (HS), and Super High Swirl (SHS) heads as shown in table 5. Additional information on the modifications to reduce friction can be found in the Appendix.

Engine	Fuel Delivery System	Compression Ratio	Principal Operating λ	Intake Valve Diameter (mm)	Flow Rate Averaged Swirl Ratio	Squish Area (%)	IVC at 10% Max Lift ABDC (°)	EPA Weighted BSFC (lbs/hp-hr)	Best BTE	Meets Emission Standard
Engine 0	Single Venturi 4 runner Manifold	9.3:1	1.0	37.6	2.08	12.3	24.5	0.7283	29.4% at 84.8 ft-lbf	YES
Engine 1 (LS)	Single Venturi Pre-Chamber Manifold	12.2:1	1.26	31.75	0.38	18.4	24.5	0.5690	37.2% at 75 ft-lbf	NO
Engine 2 (HS)	Single Venturi Pre-Chamber Manifold	12.2:1	1.44	31.75	1.5	18.4	24.5	0.5640	35.9% at 70.1 ft-lbf	NO
Engine 3 H.E. (SHS)	Single Venturi Pre-Chamber Manifold	12.7:1	1.63	37.6	3.2	36	18.5	0.5331	37.5% at 64.3 ft-lbf	NO
Engine 3 M.E. (SHS)	Single Venturi Pre-Chamber Manifold	12.7:1	1.63*	37.6	3.2	36	18.5	0.5420	36.5% at 62.8 ft-lbf	YES

Table 5: Specifications of Tested Cylinder Heads[1]

Great care and detail went into the development of each of these heads as additional augmentation of the flame speed was needed to compensate for slow flame speed the lean operation. The three heads tested were all tested using the same engine block. New head gaskets were used after each swap to avoid wear and tear from these constant interchanging of heads. Modifications in the fuel delivery system were done in an effort to reduce the cylinder to cylinder distribution in the air-fuel ratio. Also, changes made in the timing of the intake valve closing helped to increase volumetric efficiency.

[1] λ decreased at light loads to meet the required emission standards in the final engine

In the first head (Low swirl), changes to the amount of swirl was achieved without having to vary the surface area, percent of squish, or the compression ratio by rotating the combustion chamber 9° at the cylinder head gasket surface. The combustion chamber in the first head was situated in the position where it would make a 65° degree angle with the chamber wall near the intake valve and the surface of the head gasket. Rotating the combustion chamber served only to move the chamber wall nearer to the intake valve. The 9° rotation brought the wall 1.14 mm from the intake valve head and parallel to its valve stem. This modification created more swirl especially at lower valve lifts. The other head was constructed with a higher compression. Thus, the combustion chamber volume for these heads was reduced.

The stock engine head had a compression ratio of 9.3:1 and a 12.3% squish area. It produced max brake thermal efficiency (BTE) of 29.4% with a stoichiometric mixture. The stoichiometric mixture was required to allow the use of a 3 way catalyst. The flow rate averaged swirl ratio for the stock engine was 2.08. For the low swirl head, a compression ratio of 12.2:1 and an 18.4% squish area were used. The increase in compression ratio from 9.3:1 was used both to increase fuel efficiency and reduce time losses. This head is shown below in figure 5.

Figure 5: Combustion Chamber of Low Swirl Cylinder Head

The average swirl ratio was for this head was .38. Thus, this head had a relatively small amount of swirl and used mostly squish to augment the flame speed. Maximum BTE for this head was 37.2% at an air-fuel ratio of 1.26. This showed significant improvements in BTE over the stock engine. However, times losses increased substantially if lean mixture operation was attempted. Thus, it was decided to test another head with more swirl to improve on these time losses and also to improve BTE.

The second head tested simply employed a larger swirl ratio while the compression ratio and squish area remained the same. This head is shown in figure 6.

Figure 6: Combustion Chamber of High Swirl Cylinder Head

Max BTE for this head was 35.9% at an air-fuel ratio of 1.44. The average swirl ratio for this head was 1.5. It did show improvements in BTE at light loads as expected. It also produced best efficiency much leaner than the previous head. This added air-fuel ratio was used to increase fuel efficiency as it produces a higher ratio of specific heats and also by decreases the pumping mean effective pressure.

Also, testing with large spark advances showed the compression ratio could be raised without the risk of knock. Optimization of the combustion chamber geometry was important because in the case of increasing compression ratio, the potential of knocking is also increased because the end-gas temperature is increased with a rise in cylinder pressure (Mizushima).

With all of the information gained from the previous heads, a third and final head was tested with a compression ratio of 12.7:1 and a squish area of 36%. This head is shown in figure 7.

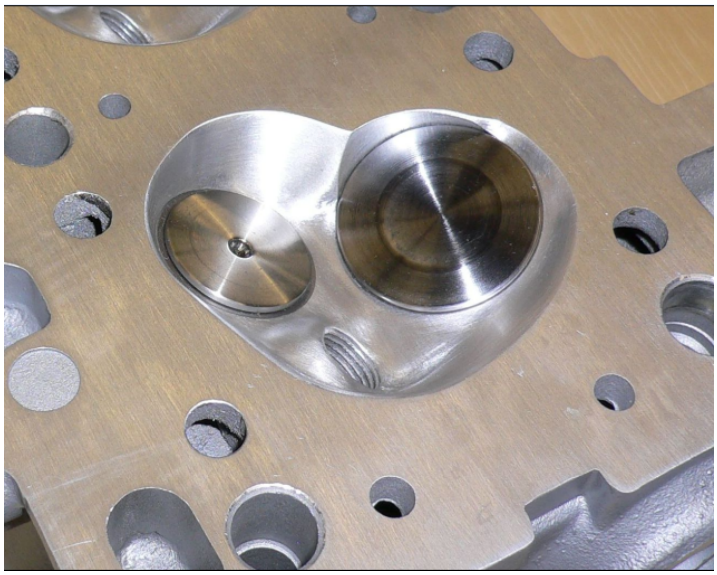

Figure 7: Combustion Chamber of Super High Swirl Cylinder Head

The swirl was also more than doubled with a swirl ratio of 3.2. These modifications produced the highest BTE among all of the heads tested. It gave a max BTE of 37.5% at an extremely lean air-fuel ratio of 1.63. Since this engine produced the highest efficiency, it was next essential to assess whether it would meet emission standards. Since this engine failed to comply with emission standards, more modifications had to be made to allow for sale in the United States.

Only two differences existed between the third and fourth engines. First, the air-fuel ratio had to be decreased to a richer mixture at lighter loads to meet the emission standards. Secondly the spark needed to be retarded from Best Efficiency Spark Advance. This resulted in a slight drop in efficiency producing a max BTE of 36.5%. Although this engine suffered a loss in efficiency from its previous modification, it is still significantly higher than the max BTE of the stock engine.

Chapter 4

Analysis and Results

The fundamental question that this research sought to answer was whether the third and most efficient engine that was previously developed could be operated so that it would meet emissions standards and still give better efficiency than the second engine developed. The purpose was to determine if an emission modified version of the third engine might be more appropriate for sale in the United States than a modified version of the second engine.

Figure 8 depicts brake thermal efficiecies of all the engines produced. It shows significant improvements in efficiency for all modifications made to the stock engine. Also, notable improvements in efficiency can be observed in the third engine over the second engine especially at light loads.

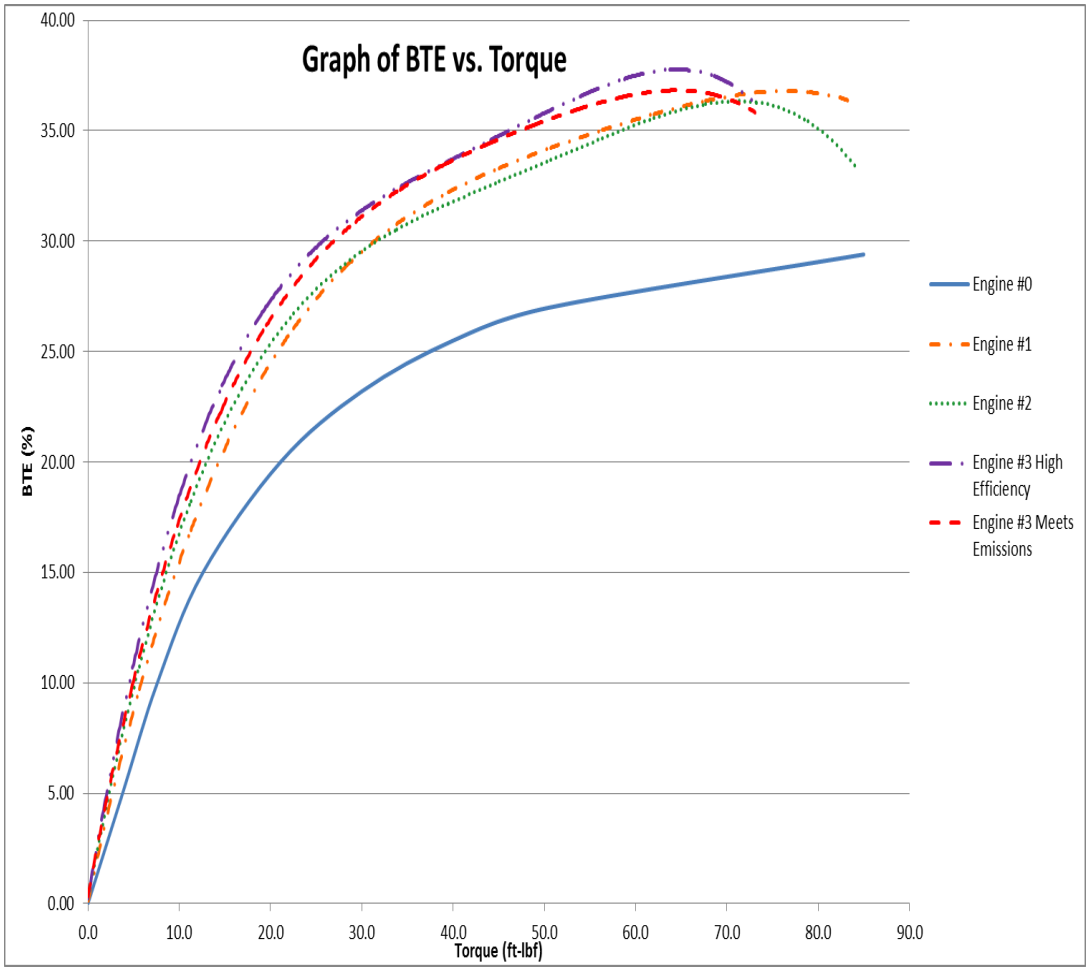

Figure 8: Graph of Brake Thermal Efficiency vs. Torque for all engines produced

The third engine was modified to meet emissions standards by altering the spark advance and air-fuel ratio. With these modifications to the operating points of the third engine, a slight drop occurred in efficiency. Although some efficiency was lost, figure 8 shows that the modified engine 3 still operates more efficiently than the second engine.

Table 6 lists the efficiency of each engine tested for each of the EPA required data points. The values of BTE were pulled directly from the generated torque curves in figure 8 and used to calculate the EPA required weighted brake specific fuel consumption (BSFC). A reduction in BSFC depicts an increase in efficiency because it means that the engine is producing more power with less fuel. This is seen here with each modification

to the previous engine. However, for engine 3 approximately 1.7% of BSFC had to be given up to meet emission standards. Although some efficiency was lost, engine 3 still had about 4.1% better BSFC than engine 2 and roughly 34.4% better BSFC than the stock engine.

Engine 3 High Efficiency			Engine 3 Meets Emisisons			Engine 2			Engine 1			Engine 0		
Torque	BTE	BSFC	Torque	BTE	BSFC	Torque	BTE	BSFC	Torque	BTE	BSFC	Torque	BTE	BSFC
ft-lbf	%	lbs C_3H_8/hp-hr	ft-lbf	%	lbs C_3H_8/hp-hr	ft-lbf	%	lbs C_3H_8/hp-hr	ft-lbf	%	lbs C_3H_8/hp-hr	ft-lbf	%	lbs C_3H_8/hp-hr
73.3	36.3137	0.5331	73.3	35.9472	0.5420	73.3	35.8917	0.5640	73.3	37.1461	0.5690	73.3	28.5685	0.7283
54.975	36.7892		54.975	36.172		54.975	35.1908		54.975	35.1769		54.975	27.2573	
36.65	33.2098		36.65	33.0977		36.65	31.067		36.65	31.2646		36.65	24.7301	
18.325	25.8683		18.325	24.8634		18.325	24.2726		18.325	23.3028		18.325	18.4535	
7.3	14.9596		7.3	14.5276		7.3	13.4683		7.3	11.9187		7.3	9.0915	
1	2.62		1	2.62		1	1.98019		1	1.71658		1	1.30355	

Table 6: Efficiency Data

The following table reports the points at which the engine had to be tested to demonstrate compliance with emission standards as required by the EPA. Both engines prove to be significantly below the 610 g/kw-hr standard for CO. This was expected as CO is usually minimal in lean operation. More CO is seen in the engine modified to meet emissions standards because a richer mixture had to be used which increases the amount of CO.

The high efficiency engine fails to meet the standard of 8 g/kw-hr for the combination of HC and NO_x. By varying spark advance and air-fuel ratio, table 6 conveys that this engine can still be operated efficiently to meet emissions standards.

Engine 3 High Efficiency					Engine 3 Meets Emissions				
Torque	HC+Nox	CO	e_{HC+NOx}	e_{CO}	Torque	HC+Nox	CO	e_{HC+NOx}	e_{CO}
ft-lbf	g/Kw-hr	g/Kw-hr	g/Kw-hr	g/Kw-hr	ft-lbf	g/Kw-hr	g/Kw-hr	g/Kw-hr	g/Kw-hr
73.3	10.981	3.915	11.8535	3.887	73.3	7.55377	3.941	7.85967	4.414
54.975	12.4326	3.679			54.975	7.83875	4.270		
36.65	10.647	3.479			36.65	7.6855	4.034		
18.325	14.4345	4.191			18.325	8.6467	4.878		
7.3	25.5521	9.396			7.3	16.9543	12.755		
1	91.31	42.705			1	91.31	42.705		

Table 7: Emissions Compliance Data

Figures 9, 10, and 11 show the effects of varying the air-fuel ratio and spark advance on brake thermal efficiency at different loads. In terms of spark advance, these graphs show that the efficiency of the engine increases as the spark is advanced more and more, reaches a maximum, and then decreases as it continues to advance. The point at which spark advance produces maximum efficiency is considered the optimum spark timing. At optimum spark timing, the maximum possible average expansion ratio is achieved. This was important to find because if the spark timing was set before this point, more work would be added to the compression stroke producing losses in efficiency. If it were to be set after this point, there would not be as much expansion of gases and again a loss in efficiency would occur. Thus, finding the optimum spark timing was critical to creating the highest possible brake thermal efficiency.

At low loads (figure 9), differentiations from the trend previously described was observed. Here, $\lambda = 1.5$ is more efficient than $\lambda = 1.63$. This phenomenon was explained by the fact that at low loads more residuals are mixed in which begin to slow down the combustion process so much that the increase in time losses are too excessive to overcome the advantage gained in reduced heat losses from lean operation.

At 39.8 ft-lbf (figure 11), for $\lambda = 1.5$ it is clear that data started to be taken at the optimum spark advance and then began to decrease. Also in figure 11, for $\lambda = 1.63$ it was

also apparent where optimum spark timing had occurred. Thus, no data was taken after that point.

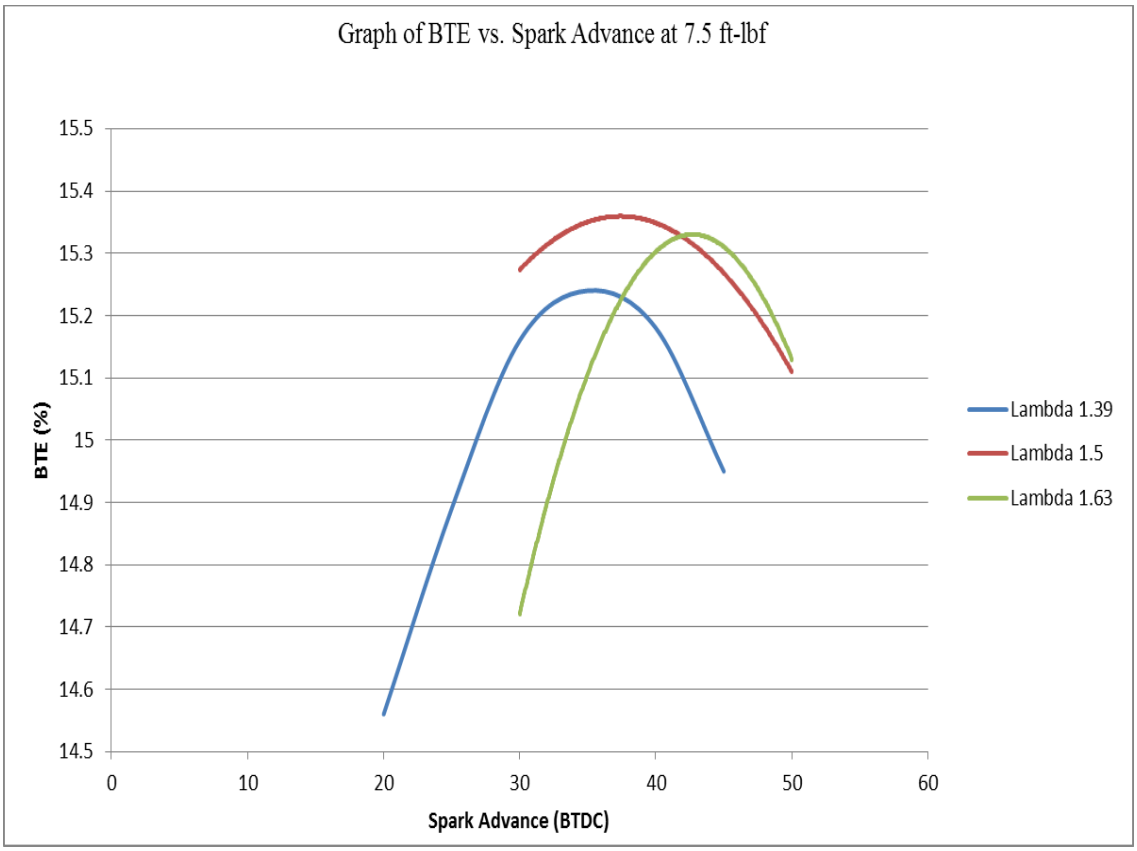

Figure 9: Effects of varying spark advance and air-fuel ratio at 7.5 ft-lbf

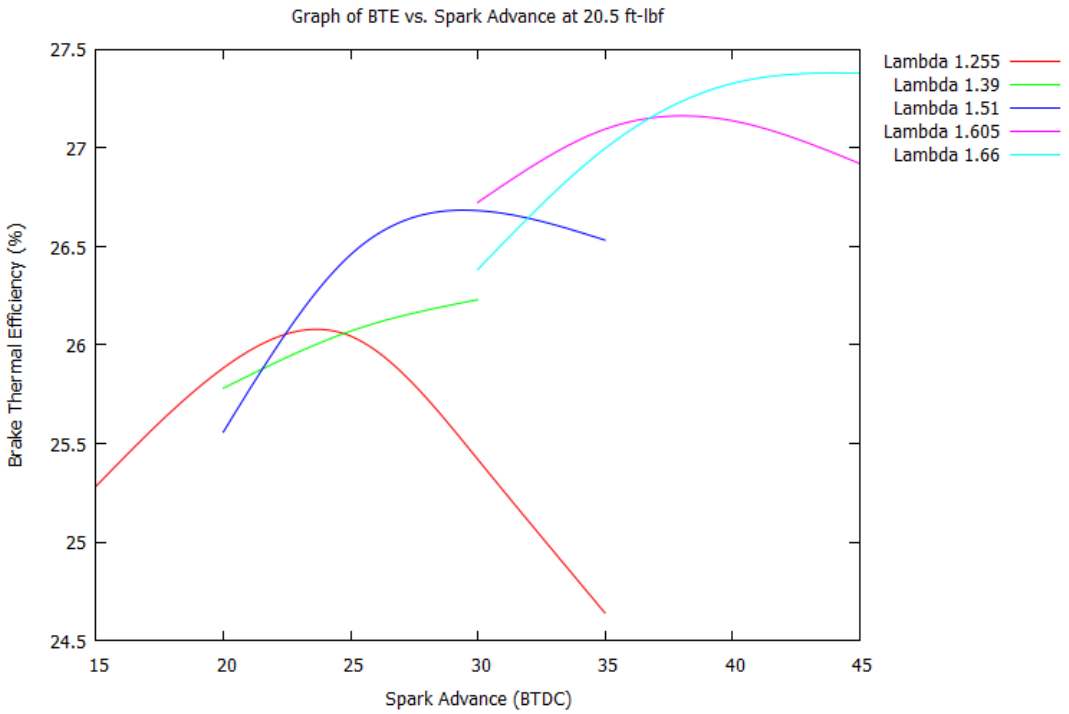

Figure 10: Effects of varying spark advance and air-fuel ratio at 20.5 ft-lbf

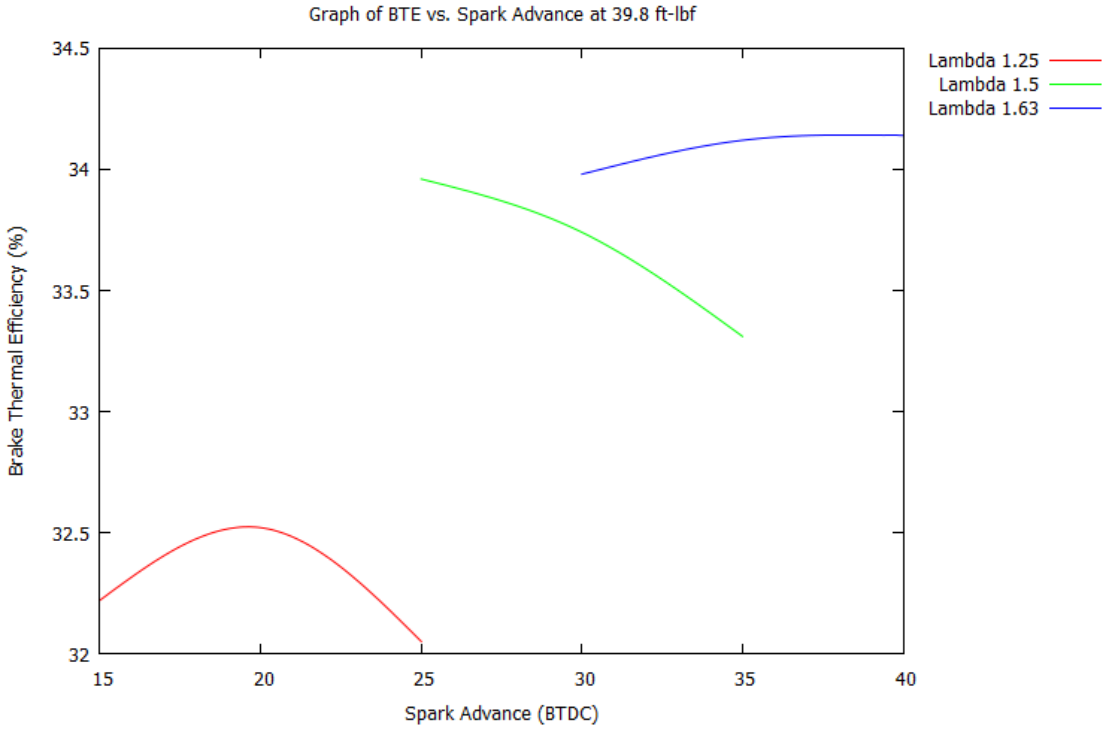

Figure 11: Effects of varying spark advance and air-fuel ratio at 39.8 ft-lbf

In terms of air-fuel ratio, figures 10 and 11 show that efficiency increases as the mixture gets leaner except at light loads when higher residuals are present. This was expected as lean operation lowers the temperature of the entire cycle by minimizing the temperatures of the working fluids and gives a better ratio of specific heats which correlates to an increase in efficiency as mentioned in the design consideration section.

Figure 12 describes the effects of spark advance and air-fuel ratio on NO_x. Here, the general trend is that NO_x increases as the spark is advanced. This is because as spark advance is added the mixture spends more time at high temperatures. Thus, more NO_x is formed since it primarily increases with temperature. The graph also shows minimal formation of NO_x for lean operation.

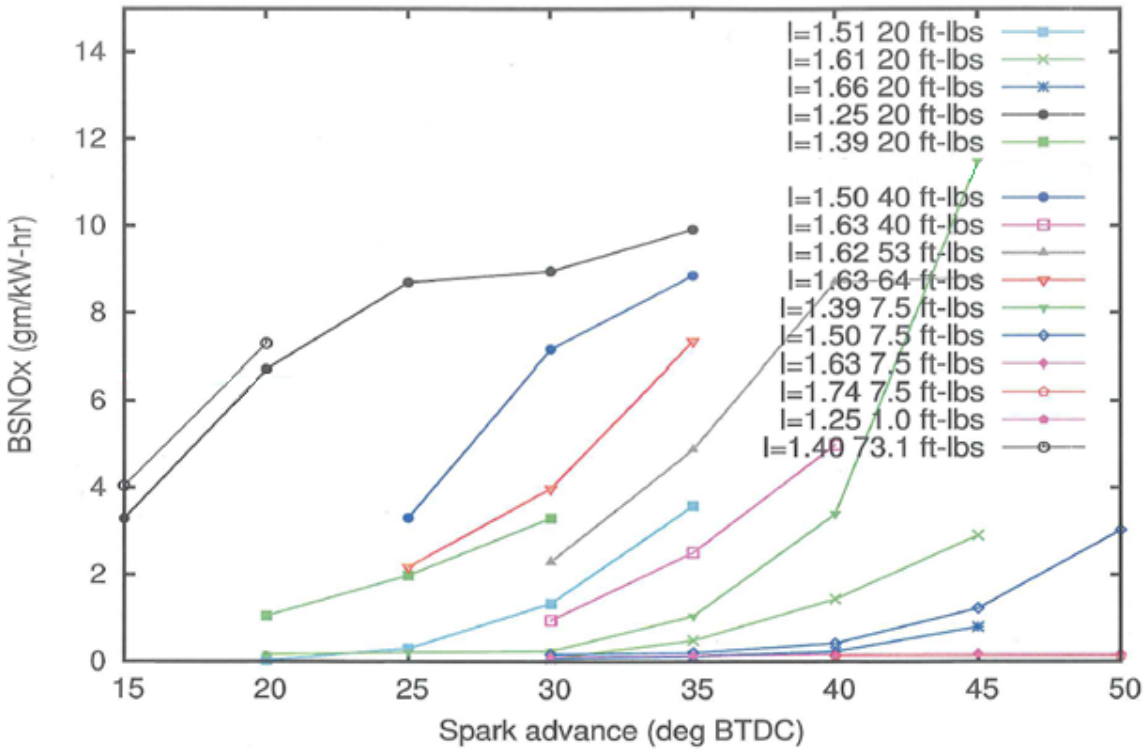

Figure 12: Effects of varying spark advance and air-fuel ratio on NOx

Figure 13 describes the effects of spark advance and air-fuel ratio on HC. It shows that HC formation can be reduced by retarding the spark for rich mixtures. In the leaner

mixtures retarding the spark produces more HC. At λ = 1.39 for both 20 ft-lbs and 7.5 ft-lbs, retarding the spark has no effect on HC formation. This is because at this point the exhaust gas temperature is not high enough to oxidize the HC.

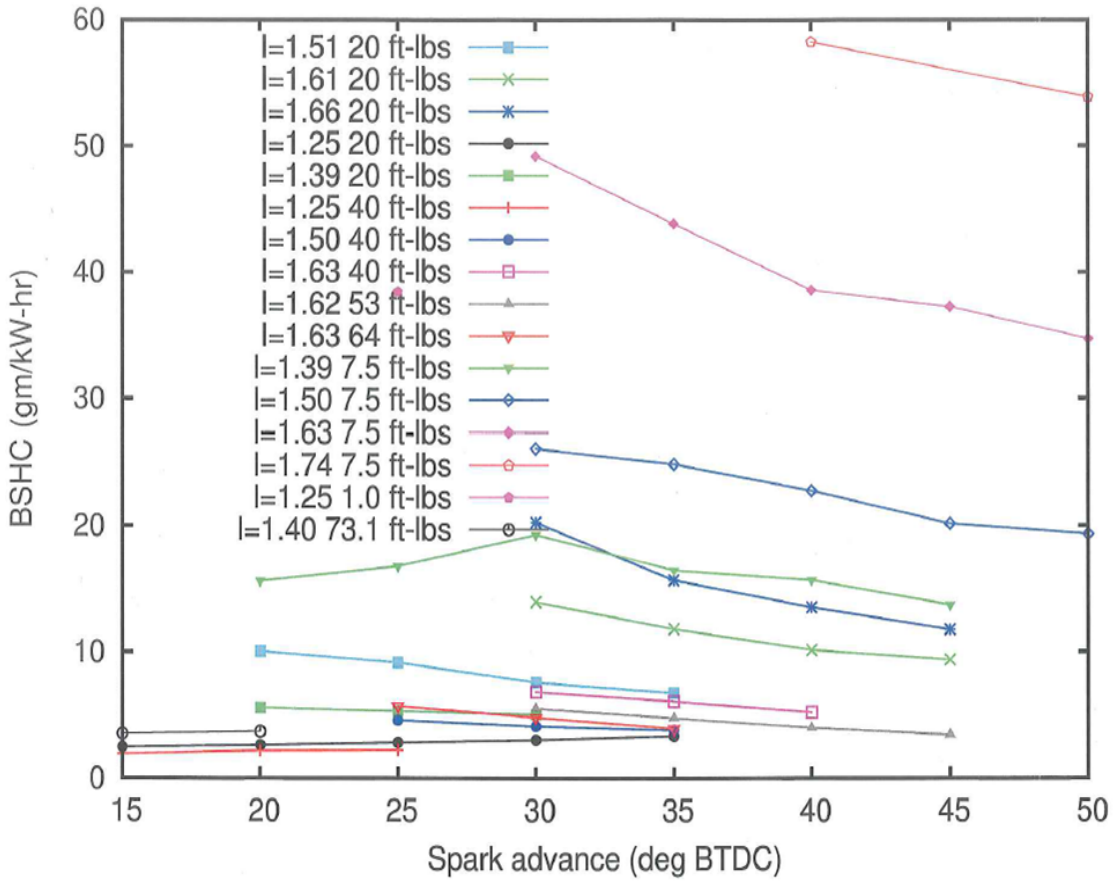

Figure 13: Effects of varying spark advance and air-fuel ratio on HC

The previous two graphs present contradictions as to where the third engine developed can be operated to meet emissions standards. On one hand, the best way to produce a minimal amount of HC is to use a rich mixture and retard the spark as much as possible. Then on the contrary, reduction of NO_x formation favors lean operation with a retarded spark. Retarding the spark prevents the engine from hitting the higher peak temperatures and generates a lower expansion ratio which results in a hotter exhaust gas temperature. Less NO_x comes from not hitting the higher peak temperatures and with a

hotter exhaust gas temperature the HC continues to be oxidized resulting in less emissions overall. However, this has to be above a given threshold level.

Figure 14 was constructed combining HC and NO_x emissions to determine the best operating point to meet the standard. This graph shows that when the mixture is extremely lean ($\lambda = 1.74$) retarding the spark produces more emissions. Richening up the mixture a bit, retarding the spark serves to help to reduce the HC creating a significant decrease in overall emissions.

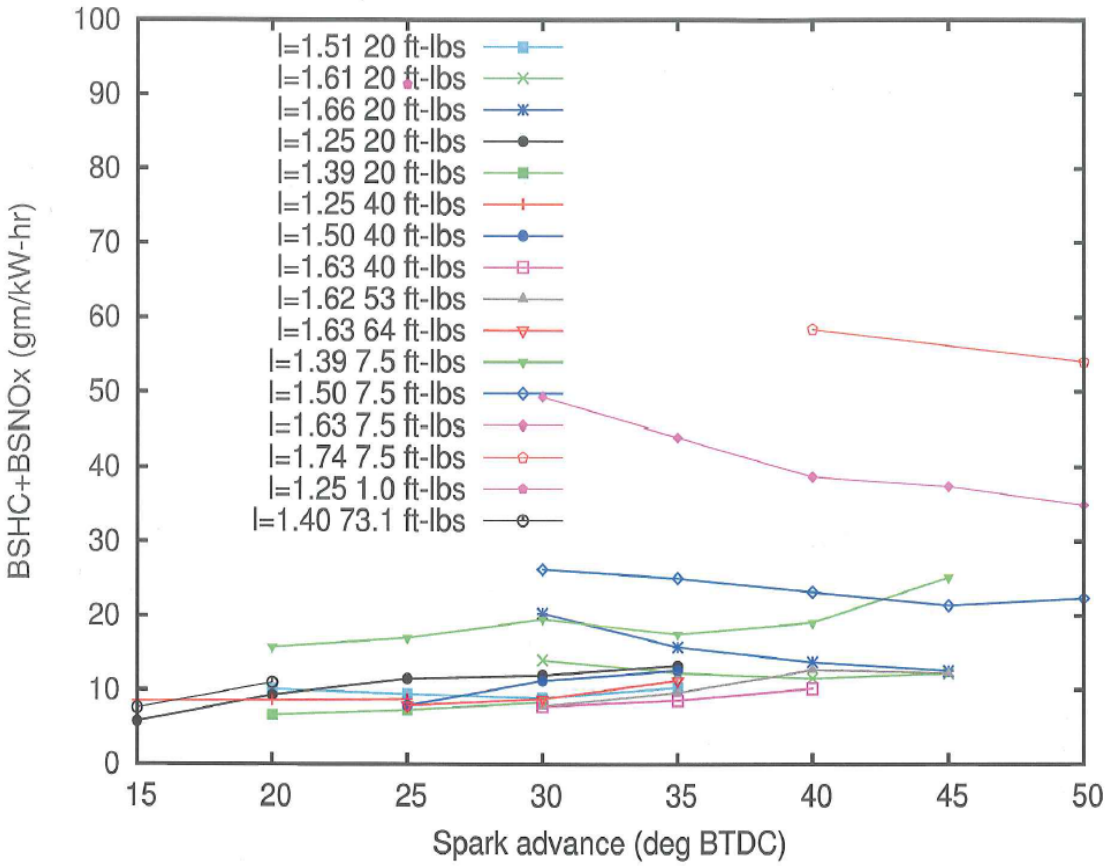

Figure 14: Effects of varying spark advance and air-fuel ratio on HC and NOx

The effects of varying the spark advance and air-fuel ratio were not evaluated for CO emissions in this research. This was because CO was not expected to be problematic

since the engine would be run extremely lean. This proved to be precise and results for CO emissions are shown above in table 6.

Chapter 5

Conclusions

1. A high efficiency engine could be produced cheaply and operated as a generator showing improvements of 36.8% in EPA cycle BSFC over the stock engine.
2. This high efficiency engine could be modified to meet emissions standards by making adjustments to spark advance and air-fuel ratio.
3. It was able to meet emissions standards without the added cost of a catalyst or a computer to control the air-fuel ratio to ensure that the catalyst does not alter emissions by orders of magnitude.
4. This research also proved that previous developments of this engine would not need to be tested for emissions as this final modification was still more efficient than any of the previous engines, deviating approximately 1.7% from the highest efficiency engine.
5. Since this engine met EPA regulations, it could be sold both in the United States and abroad.

References

Baker, Paul, and Harry Watson. MPI Air/Fuel Mixing for Gaseous and Liquid LPG. SAE Paper 2005-01-0246. University of Melbourne, 2005.

Bishop, I. Effect of Design Variables on Friction and Economy. SAE Paper 640807. 1964.

Clean Air Technology Center. Nitrogen Oxides (NOx), Why and How They Are Controlled. EPA-456/F-99-006R, Environmental Protection Agency, November 1999.

"Control of Emissions from New, Small Nonroad Spark-Ignition Engines and Equipment." Code of Federal Regulations. Environmental Protection Agency.

Daniel, W. A. Engine Variable Effects on Exhaust Hydrocarbon Composition (A Single-Cylinder Engine Study With Propane as the Fuel). SAE Paper 670124. General Motors, 1967.

"Engine Testing Procedures." Code of Federal Regulations. Environmental Protection Agency.

Engineering Toolbox. "Actual Air Compressor Capacity (ACFM) versus Standard Air Capacity (SCFM) and Inlet Air Capacity (ICFM)." SCFM versus ACFM and ICFM.

Engineering Toolbox. "Density of Dry Air, Water Vapor and Moist Humid Air.

Mizushima, Norifumi, Susumu Sato, Yasuhiro Ogawa, Toshiro Yamamoto, Umerujan Sawut, Buso Takigawa, Koji Kawayoko, and Gensaku Konagai. Combustion Characteristics and Performance Increase of an LPG-SI Engine with Liquid Fuel Injection System. SAE Paper 2009-01-2785. 2009.

Quader, Ather A. Lean Combustion and the Misfire Limit in Spark Ignitiion Engines. SAE Paper 741055. General Motors, 1974.

Samarajeewa, Hasitha. Design of 1.6L Genset Engine. Thesis. University of Miami, 2011.

Stone, Richard. Introduction to Internal Combustion Engines. Warrendale, PA: Society of Automotive Engineers, 1999.

Appendix

Meriam 40OHE35WM Inclined Manometer

Meriam 50 MC2-2P Laminar Flow Element

Superflow D-516 Water-brake Dynamometer

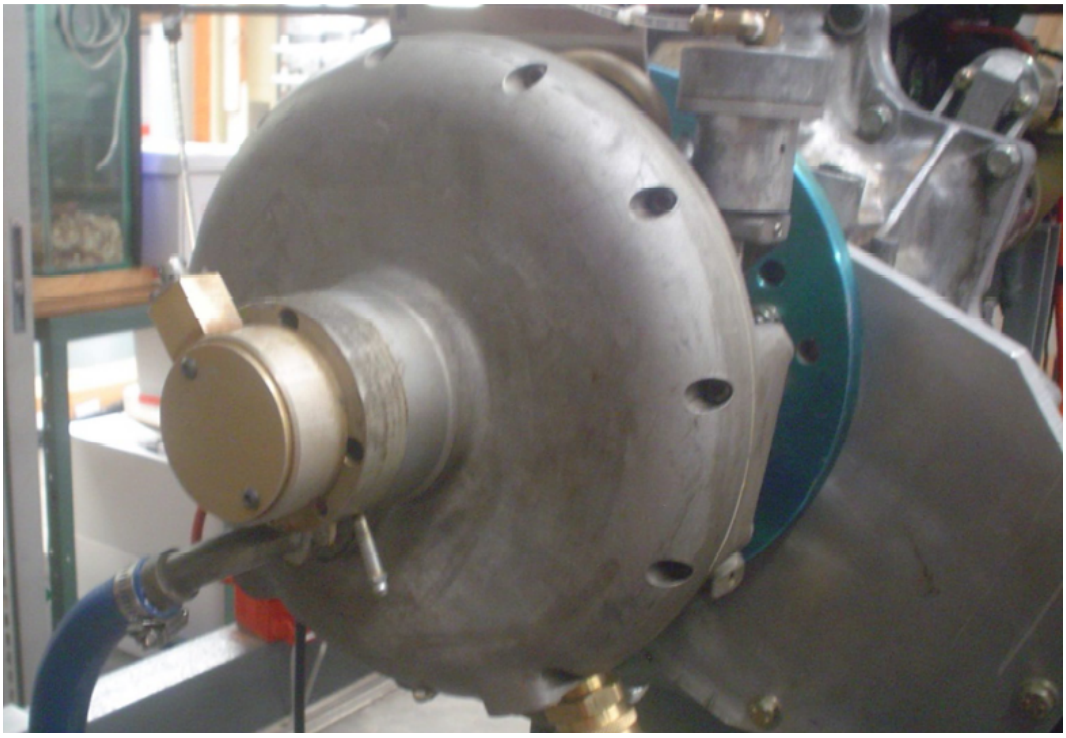

Ametek Digistrobe III 1965

Omegaclad Thermocouples

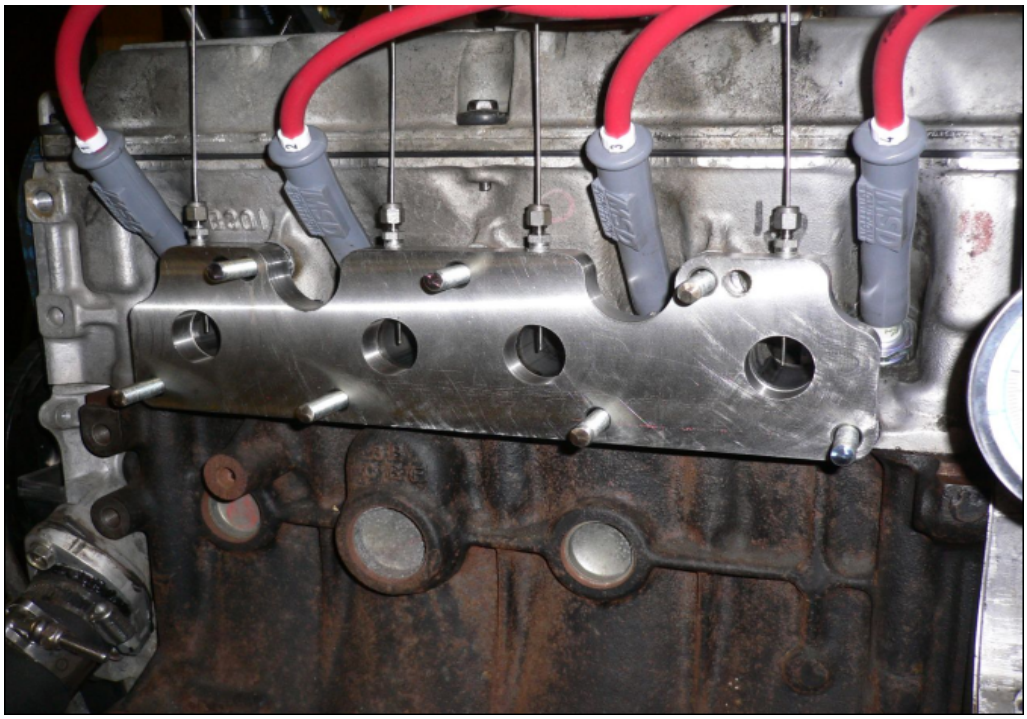

Ferrett 16 Gas Link II NDIR Gas Analyzer

Engine History Chart

Engine	Fuel Delivery System	Compression Ratio	Principal Operating λ	Intake Valve Diameter (mm)	Flow Rate Averaged Swirl Ratio	Squish Area (%)	IVC at 10% Max Lift ABDC (°)	Crank Shaft Journal Diameter (mm)	Valve Spring Force Closed/ Open (lbs)	Piston and Rings Diameter (mm) Weight (gr) Ring Width	Connecting Rod Length (mm) Weight (gr)	EPA Weighted BSFC (lbs/hp-hr)	Best BTE	Meets Emission Standard
Engine 0	Single Venturi 4 runner Manifold	9.3:1	1.0	37.6	2.08	12.3	24.5	45/50	42 115	78 298.3 1.5x1.5x4.0	132.9 519.6	0.7283	29.4% at 84.8 ft-lbf	YES
Engine 1 (LS)	Single Venturi Pre-Chamber Manifold	12.2:1	1.26	31.75	0.38	18.4	24.5	40/49	42 115	79 280.0 1.0x1.2x2.8	138.4 418.0	0.5690	37.2% at 75 ft-lbf	NO
Engine 2 (HS)	Single Venturi Pre-Chamber Manifold	12.2:1	1.44	31.75	1.5	18.4	24.5	40/49	42 115	79 280.0 1.0x1.2x2.8	138.4 418.0	0.5640	35.9% at 70.1 ft-lbf	NO
Engine 3 H.E. (SHS)	Single Venturi Pre-Chamber Manifold	12.7:1	1.63	37.6	3.2	36	18.5	40/49	24 51	79 280.0 1.0x1.2x2.8	138.4 418.0	0.5331	37.5% at 64.3 ft-lbf	NO
Engine 3 M.E. (SHS)	Single Venturi Pre-Chamber Manifold	12.7:1	1.63*	37.6	3.2	36	18.5	40/49	24 51	79 280.0 1.0x1.2x2.8	138.4 418.0	0.5420	36.5% at 62.8 ft-lbf	YES